Constitutive Relations for Reactive Transport Modeling: Effects of Chemical Reactions on Multi-Phase Flow Properties

Shuo Zhang[a,*], Hui-Hai Liu[a], Marinus I.J. van Dijke[b], Sebastian Geiger[b], Susan M. Agar[a]

[a] *Aramco Research Center-Houston, 16300 Park Row Dr. Houston, TX, 77084*
[b] *Heriot-Watt University, Edinburgh, EH14 4AS, United Kingdom*

Abstract

The relationship between flow properties and chemical reactions is key to modeling subsurface reactive transport. This study develops closed-form equations to describe the effects of mineral precipitation and dissolution on multiphase flow properties (capillary pressure and relative permeabilities) of porous media. The model accounts for the fact that precipitation/dissolution only takes place in the water-filled part of pore space. The capillary tube concept was used to connect pore-scale changes to macroscopic hydraulic properties. Precipitation/dissolution induces changes in the pore radii of water-filled pores and consequently in the pore-size distribution. The updated pore-size distribution is converted back to a new capillary pressure-water saturation relation from which the new relative permeabilities are calculated. Pore network modeling is conducted on a Berea sandstone to validate the new continuum-scale relations. The pore network modeling results are satisfactorily predicted by the new closed-form equations.

Keywords: Mineral reactions, multiphase flow properties, reactive transport, constitutive relations

1. Introduction

In order to model geochemical reactions together with subsurface flow and solute transport, reactive transport modeling (RTM) is receiving increasing interest (Steefel et al., 2005). RTM refers to the creation of computer models that integrate chemical reactions with the transport of fluids through the Earth's crust. Such models predict the distribution in space and time of the chemical reactions that occur along a flow

*Corresponding author
Email address: shuo.zhang@aramcoservices.com (Shuo Zhang)

path. Today, RTM has become an essential tool for the analysis of coupled physical, chemical, and biological processes in Earth systems. The advantage of this approach is that it links individual time- and space-dependent processes in complex natural systems.

In order to model hydro-geochemical problems on a large scale, RTM employs continuum representations of the porous medium and assumes the existence of a representative elementary volume where, for instance, flow can be described by Darcy's law (Steefel et al., 2005). A porous medium is treated as continuous domains with macroscopic flow and transport parameters such as hydraulic conductivity, porosity, dispersivity, as well as geochemical parameters such as reactive surface area and reaction rates. However, geochemical reactions such as mineral dissolution/precipitation modify the porous medium's pore structure. An up-scaling procedure is needed to predict changes in hydraulic properties such as permeability, capillary pressure, and relative permeabilities within the framework of continuum-scale flow and transport models.

Currently the effects of chemical reactions on flow properties are represented as a relation between permeability and porosity in reactive transport modeling. Porosity is updated after chemical calculations from the change of mineral volumes, then permeability change is calculated from the porosity change using an empirical permeability-porosity relation, most commonly the Carman-Kozeny relation (Kozeny, 1927; Carman, 1956), or the Verma and Pruess (1988) relation. To the best of our knowledge, there are no closed-form relations available yet for the effects of chemical reactions on multi-phase flow properties, and thus currently these effects cannot be accounted for in reactive transport modeling.

This paper presents new constitutive relations to represent how chemical reactions affect multi-phase flow properties on the continuum scale based on the conceptual model of parallel capillary tubes. The parameters in our new relations are either pre-existing input in a multi-phase flow simulation (initial capillary pressure function), or intermediate modeling results (water saturation, changes in mineral volume). With those parameters the new relations can be implemented in an existing reactive transport simulator directly, without introducing new variables.

The change of porosity, permeability, and multi-phase flow parameters due to mineral reactions in a porous medium can be caused by different mechanisms in different scenarios. For example, Pruess and Müller (2009) investigate permeability change due to salt precipitation in the context of CO_2 injection. The rational for this process is that during CO_2 injection, water evaporates into the CO_2 stream. Salinity starts to increase in the water and salt eventually precipitates out. Pruess and Müller (2009) discuss how this 'dry out' will impact injectivity by modeling the permeability change due to salt precipitation. Reduction of permeability can also be a consequence of bacterial growth in a porous medium as a consequence of groundwater

recharge, water treatment or disposal processes, enhanced oil recovery schemes, or in-situ bioremediation of organic contaminants in groundwater (Taylor and Jaffé, 1990; Ginn et al., 2002; Schäfer et al., 1998). Plugging can be particularly severe for water injection and bioremediation projects, since both processes inject water containing relatively high levels of growth substrate and inorganic nutrients.

Mineral dissolution occurs where acid reacts with the surfaces of a porous medium. A common method of stimulating oil wells to achieve greater production is to inject acid into an oil bearing formation with the hope of significantly increasing the permeability in some region around the wellbore. The reacting acid will dissolve a portion of the porous solid thus changing the pore structure. The extent to which this dissolution of solid enhances permeability of the reservoir is essential to the design of an effective acid treatment (Schechter and Gidley, 1969; Hiorth et al., 2010).

The relation between porosity change and permeability change is also relevant to the effects of diagenesis such as cementation or dissolution on reservoir quality prediction. Depending on the chemical and crystallographic properties, cements fill the intergranular pores and increase the tortuosity of the permeable medium. The result is a reduction in permeability compared to unaltered rock. The uncertainty of the location and chemical composition of various cements makes it difficult to predict their effects on permeability (Panda and Lake, 1995; Bjørkum and Nadeau, 1998).

This paper is intended to provide the fundamental basis for making reliable estimates of the influence of pore structure on multi-phase flow properties. Our approach should yield results pertinent to the problems cited above. Indeed, any problem concerned with interaction of the porous solid-fluid system and its effects on multi-phase flow properties should be susceptible to arguments similar to these presented here.

2. Previous Relations

Mineral dissolution and precipitation reactions in subsurface porous media alter the structure of the pore network. The changes in pore structure manifest themselves in the constitutive relations that characterize the continuum-scale properties of the medium and are used in the governing equations of flow and transport. The question is how these effects can be accurately captured in modeling reactive transport in reservoirs.

The porosity changes caused by mineral reactions can be easily related to precipitation or dissolution volume, but the permeability change associated with a change in porosity is a more complex problem, as the porosity-permeability correlations depend on many geometric factors such as pore-size distribution, pore shapes, and connectivity. Since there is a wide variation in these geometric properties among natural rock formations, the porosity-permeability correlations will generally depend on the rock type and will be site specific. Attempts to obtain this relationship by many

investigators have produced results which differ considerably from each other. For example, Mavis and Wilsey (1937) found the permeability of filter sands to be proportional to ϕ^5 or ϕ^6, while Brace (1977) found a 3rd power correlation with porosity for crystalline rocks. It is therefore obvious that no simple general correlation between porosity and permeability can be applied to all permeable materials. Xie et al. (2014) discusses the implementation of permeability-porosity relationship in several reactive transport codes and conducted benchmark problems, but only the Carman-Kozeny relation is used in their models.

In fact we do not need an absolute permeability-porosity correlation but the relationship between their relative changes. Many investigators have proposed such relationships for different materials in which the porosity changes were brought about by different physical mechanisms. The straight capillary models have been frequently employed. Verma and Pruess (1988) assume that the medium has a set of non-intersecting flow channels with either circular tubular or planar cross sections, and construct series of models that are able to represent pore throat effects. Minor changes in average porosity cause drastic permeability changes due to closure of the pore throats in their model, and they find that there is a non-zero critical porosity ϕ_c at which permeability reduces to zero.

The relations above assume that mineral dissolution and precipitation reactions occur in all pores and ignore the important fact that for multiphase flow, these reactions only occur in pores occupied by the water phase. For example, Ott et al. (2015) observe in their CO_2 coring flooding experiment that precipitated salt occupies complementary space with initial CO_2 gas, and the overlap between salt precipitation and initial gas overlap less than 5%. As a result, these traditional approaches are applicable to the single-phase flow condition only, while multiphase flow is common in oil and gas reservoirs, geothermal reservoirs, geological carbon storage, and groundwater remediation. Liu et al. (2013) use the concept of multi-phase flow in calculating the change of permeability due to a change in porosity. These authors argue that in multi-phase flow conditions, precipitation occurs only in the pore space occupied by brine, which corresponds to the small capillary tubes in the capillary tube model, since in most cases water is the wetting phase. They derive the relationship between permeability change and porosity change based on their conceptual model, and verify their predictions of new permeability with experimental results. However, although Liu et al. (2013) provide the relation of permeability change and chemical reactions, practical approaches to accurately estimate the effects of mineral dissolution and precipitation reactions on multiphase flow properties are not yet available.

This paper presents continuum-scale constitutive equations to calculate reaction-induced changes in capillary pressure and relative permeabilities. Section 3 presents the derivation of our new relationships. These new constitutive equations are fundamentally based on the capillary tube concept. One assumption in this concept is

that the connectivity between pores in the rocks is represented by a group of capillary tubes. To test whether this assumption will affect our predictions in changes of capillary pressure and relative permeabilities, we present pore network modeling on a Berea sandstone in Section 4 and compare the results with predictions from the new continuum-scale equations.

The pore network models provide opportunities to study the change of hydraulic properties due to reactions because detailed information is available at the pore scale (Algive et al., 2012). Raoof et al. (2013) developed a pore-network modeling tool capable of simulating fluid flow and multi-component reactive and adsorptive transport under saturated and variably saturated conditions. Other researchers (Nogues et al., 2013; Li et al., 2006; Varloteaux et al., 2013) have also developed similar reactive transport models that are able to simulate the evolution of pore bodies within a network. These models can be used to understand the evolution of porosity and permeability in porous media at the pore scale, and aid in the representation of constitutive relationships such as a porosity-permeability curve that can be used to model larger scale processes in continuum scale models. However, to account for changes in conductivity at the pore-to-pore level due to changes in the pore body volume due to precipitation or dissolution of minerals, assumptions have to be made to correlate the change in volume of the pores to a change in throat diameter. For example, in Nogues et al. (2013), it is assumed that all pore throats are cylindrical in shape and have a characteristic diameter, and mineral precipitation or dissolution simply reduces the volume of the system and preferential precipitation/dissolution effects are not taken into account. Thus the conclusions for the porosity-permeability relationship from such models are mostly determined by how the pore-diameter change is related to pore-volume change.

3. Theory Development

Our approach to derive the relation between chemical reactions and changes in capillary pressure and relative permeabilities are shown in Fig.1 and described as follows: starting with continuum-scale hydraulic properties, the pore size distribution (PSD) function is calculated from the initial capillary pressure curve using the capillary tube concept. Changes in mineral volume through equilibrium or kinetic mineral reactions are then translated to changes in pore radii of the PSD by selectively changing the radii of water occupied pores. The resulting new PSD is converted back to an updated capillary pressure curve, which is then used for computing total permeability and relative permeabilities at the continuum scale. Note that our new development is based on the Mualem (1976) or Van Genuchten (1980) model for capillary pressure and relative permeability (before chemical reactions), but the procedure can be also applied to other models.

3.1. Change in Pore Size Distribution

The pore space of a porous medium is conceptualized as cylindrical capillaries with a continuous distribution of radii r. A given capillary can be either water-filled or completely dry, depending on the saturation state of the medium. With this geometric idealization, the capillary pressure-water saturation curve can be interpreted to represent continuous cumulative pore-size distributions. In a given portion of the porous medium (in computational terms this would be a cell within the modeled domain), at any time the water content is known. Due to precipitation/dissolution, the pore volumes and pore sizes will change and thus the capillary pressure curve changes also. The maximum radius up to which pores are water-filled and therefore affected by mineral reactions can be calculated from the capillary pressure head:

$$r = \frac{\zeta}{h} \tag{1}$$

where r is the radius of capillary tubes, h is the capillary pressure head corresponding to the current effective water saturation S, and ζ is the capillary factor $\zeta = \frac{2\sigma cos\phi}{\rho g}$. Effective water saturation is defined as:

$$\bar{S} = \frac{S - S_r}{1 - S_r}, \tag{2}$$

where S is the wetting-phase saturation (the ratio of wetting-phase volume to the corresponding bulk volume of pore space), and subscript r refers to the residual water saturation.

The capillary pressure head h can be related to effective wetting-phase saturation by Van Genuchten (1980):

$$\bar{S} = [1 + (\alpha h)^n]^{-m}, \tag{3}$$

where α and *m=1-1/n* are empirical parameters.

Before mineral reactions occur, the relative permeability of the wetting phase k_r can be expressed by Mualem (1976):

$$k_r = \bar{S}^{1/2}[\frac{\int_0^{\bar{s}}(1/h(x))dx}{\int_0^1(1/h(x))dx}]^2. \tag{4}$$

Using the mathematical relation (Van Genuchten, 1980),

$$F(\bar{S}) = \frac{\int_0^{\bar{s}}(1/h(x))dx}{\int_0^1(1/h(x))dx} = 1 - (1 - \bar{S}^{1/m})^m, \tag{5}$$

we have

$$k_r(\bar{S}) = \bar{S}^{1/2}[1 - (1 - \bar{S}^{1/m})^m]^2. \tag{6}$$

The changes in pore geometry during mineral precipitation or dissolution are complex. However, in order to obtain a closed-form result, we need to make some simplifications. Here we assume a strict dependency of mineral reactions on solution concentrations. In other words, the amount of dissolved or precipitated mineral in a given pore is linearly dependent on its pore volume. Also, we assume that the change in pore volume is uniform within a given pore.

If we denote the brine saturation at the time when mineral reaction starts as S_p, then we can define the ratio of the pore volume after chemical reactions to that before reactions, β, as

$$\beta = \frac{S_p - S_{reaction}}{S_p}, \tag{7}$$

where $S_{reaction}$ is the content of precipitated or dissolved mineral, defined as the volume of mineral change divided by the bulk volume of pore space, and is positive for precipitation.

Given a porosity change from ϕ_0 to ϕ of a porous medium due to mineral dissolution or precipitation, β can be calculated as

$$\beta = 1 - \frac{(\phi_0 - \phi)/\phi_0}{S_p}. \tag{8}$$

The ratio δ of the radius (for a pore after precipitation/dissolution) to its original radius can be approximated to be a power function of the corresponding volume ratio (Liu et al., 2013):

$$\delta = \frac{r^*}{r} = \beta^\chi, \tag{9}$$

where r^* is the radius after precipitation/dissolution, r is the original radius, and χ is an empirical parameter equal to 4.5. Liu et al. (2013) discussed this power law in detail. They selected the value of 4.5 to be consistent with patchy distribution of deposits, which was observed from scanning electron micrograph study where salt crystal did not distribute uniformly within a pore, but grew inwardly. Readers are referred to the Liu et al. (2013) paper and references therein.

In the previous study by Verma and Pruess (1988), changes in mineral volume were modeled as affecting the entire pore spectrum even though mineral reactions occur only in the water-filled part of the pore space. Here we only translate changes in mineral volumes to pore radii in the wet part of the porous medium.

In a given portion of the porous medium, at any time the water saturation is known. The maximum radius up to which pores are water-filled and therefore affected by mineral reactions is calculated by combining Eq.3 and Eq.1:

$$r_p = \alpha\zeta[\bar{S}_p^{-1/m} - 1]^{-1/n}. \tag{10}$$

The radius r_p divides the pore spectrum into a dry, inert part and a wet reactive part, which compensates for the change in mineral volume. For the calculation of the new PSD, only the pore radii of the wet pore space are multiplied by the proportionality factor δ.

3.2. Capillary Pressure

The calculation of change in capillary pressure after mineral reactions is straightforward since capillary pressure is proportional to $1/r$.

Since the radius is changed from r to $r\delta$ for $S \leq S_p$ and remains unchanged for $S > S_p$, the new capillary pressure head is

$$h(S) = \begin{cases} \dfrac{h_0(S)}{\delta} & S \leq S_p \\ h_0(S) & S > S_p \end{cases}, \tag{11}$$

where h_0 is the initial capillary pressure head at saturation S. This means that capillary pressure is increased by a factor of $1/\delta$ for $S \leq S_p$ in the case of precipitation ($\delta < 1$), and unchanged for $S > S_p$. Note that the new h-S curve is not continuous at $S = S_p$. This is because that mineral precipitation/dissolution only occurs in the water phase where $S \leq S_p$.

In the case of dissolution ($\delta > 1$), the sizes of the small pores initially occupied by water increase, and can potentially become larger than the previously large pores. Thus the pores need to be rearranged in terms of pore sizes to determine the new capillary pressure curve. If we follow the approach of the precipitation case, the new curve, which is a piecewise function, will have an offset at water saturation S_p using Eq.11, as indicated by the red dashed line in Fig.2. This means that some of the low saturations (S_1 to S_p) correspond to lower capillary pressures compared to some of the high saturations (S_p to S_2), which is physically not possible in the conceptual model of capillary tubes. In fact, some pores on the left side of S_p (S_1 to S_p) have larger pore sizes than some other pores on the right side (S_p to S_2), while water will always fill the small pores first. The pores whose sizes need to be rearranged in the new capillary curve lie between two threshold saturations, S_1 and S_2, which correspond to capillary pressure heads δh_p and h_p/δ, where h_p is the capillary pressure head for

S_p in the initial capillary pressure curve. Thus, S_1 and S_2 can be calculated as

$$\begin{cases} S_1 = [1 + (\alpha h_p \delta)^n]^{-m} \\ S_2 = [1 + (\alpha h_p / \delta)^n]^{-m} \end{cases} \tag{12}$$

, where $h_p = h_0(S_p)$.

For $S < S_1$ and $S > S_2$, the new capillary pressure curve follows Eq.11. However, for $S_1 \leq S \leq S_2$, the capillary pressure curve needs to be adjusted. For a given capillary pressure head h ($h_p/\delta \leq h \leq h_p$), the water volume from h_p to h comes from two sources, the inert pores that have smaller pore radii than those corresponding to h ($\hat{S}_2$ to S_p), and the reactive pores whose sizes are enlarged but are still smaller compared to that corresponding to h ($\hat{S}_1$ to S_1). Thus,

$$S - S_1 = (\hat{S}_1 - S_1) + (\hat{S}_2 - S_p), \tag{13}$$

where $\hat{S}_1 = [1 + (\alpha h \delta)^n]^{-m}$ and $\hat{S}_2 = [1 + (\alpha h)^n]^{-m}$. Thus, the equation for the capillary pressure head after mineral dissolution is

$$S = \begin{cases} [1 + (\alpha h \delta)^n]^{-m} & h > h_p \\ [1 + (\alpha h \delta)^n]^{-m} + [1 + (\alpha h)^n]^{-m} - S_p & h_p/\delta < h \leq h_p \\ [1 + (\alpha h)^n]^{-m} & h \leq h_p/\delta \end{cases}. \tag{14}$$

The values calculated from this final equation is plotted in Fig.2 as blue dashed line, where capillary pressure is a monotone function of water saturation. Note that here water saturation is written as a function of capillary pressure head, but capillary pressure head is not an explicit function of water saturation. This prevents us from obtaining closed-form equations for relative permeabilities for the dissolution case, which will be discuss later.

3.3. Permeability

The closed-form equation for permeability change due to mineral reactions is given in Liu et al. (2013) as follows:

$$\frac{K}{K_0} = \tau^{1/2}[(\delta - 1)(1 - (1 - \bar{S}_p^{1/m})^m) + 1]^2, \tag{15}$$

where τ is the tortuosity factor, and $\tau = 1 - \bar{S}_p + \delta^2 \bar{S}_p$. Liu et al. (2013) define this tortuosity factor to account for the fact that precipitated minerals impact tortuosity of porous media. This definition allows the tortuosity factor to have desirable values in two important cases: one for $\delta = 1$ (without precipitation) and $(1 - \bar{S}_p)^{1/2}$ for $\delta = 0$

Here we derive this relation using the pore size distribution (PSD) function $f(r)$, which will give us a slightly different result. The PSD function can be expressed by differentiation of the cumulative water content with respect to r (Ritter and Drake, 1945). Before chemical reactions,

$$f(r) = \frac{d\theta(r)}{dr}. \tag{16}$$

We denote the new PSD function as $f^*(r^*)$, the new water content as θ^*, and the new radius as r^*. Recall that we defined the volume ratio before and after reactions as β, and the radius ratio as δ. Thus, we have $\theta^* = \theta\beta$, $r^* = r\delta$. For $r < r_p$, the new PSD function is

$$f^*(r^*) = \frac{d\theta^*(r^*)}{dr^*} = \frac{\beta}{\delta} f(\frac{r^*}{\delta}). \tag{17}$$

Following Liu et al. (2013), only the water occupied pores are modified,

$$\frac{K}{K_0} = \tau^{1/2}[\frac{\int_0^{r_p^*} r^* f^*(r^*) dr^* + \int_{r_p}^{\infty} r f(r) dr}{\int_0^{\infty} r f(r) dr}]^2, \tag{18}$$

where r_p is the threshold radius below which pores are occupied by water, and $r_p^* = r_p\delta$, which is the threshold radius post mineral reaction.

Substituting Eq.17 into Eq.18, we have

$$\frac{K}{K_0} = \tau^{1/2}[\frac{\int_0^{r_p} \delta\beta r f(r) dr + \int_{r_p}^{\infty} r f(r) dr}{\int_0^{\infty} r f(r) dr}]^2. \tag{19}$$

Using the mathematical relation (Van Genuchten, 1980),

$$F(\bar{S}) = \frac{\int_0^{r} r f(r) dr}{\int_0^{\infty} r f(r) dr} = 1 - (1 - \bar{S}^{1/m})^m, \tag{20}$$

we obtain

$$\frac{K}{K_0} = \tau^{1/2}[(\delta\beta - 1)(1 - (1 - \bar{S}_p^{1/m})^m) + 1]^2. \tag{21}$$

Comparing Eq.21 with Eq.15, the only difference is that Liu et al. (2013) misses a β term.

3.4. Relative Permeability of Water

Relative permeabilities are defined as the permeability of one phase divided by the saturated permeability, in our case, the saturated permeability of modified porous medium (K). However, for simplicity, we derive our new relative permeabilities as divided by the saturated permeability of the original porous medium (K_0). These relations can be corrected simply by using the factor K/K_0 as expressed in Eq.21. Let us denote the initial water permeability as K_{w0}, relative permeability as k_{w0}, and the new water permeability as K_w, relative permeability as k_w. Following Mualem (1976), we obtain

$$k_{w0} = \frac{K_{w0}}{K_0} = \tau^{1/2}[\frac{\int_0^r rf(r)dr}{\int_0^\infty rf(r)dr}]^2 = \tau^{1/2}[F(\bar{S})]^2, \tag{22}$$

where $\tau = \bar{S}$.

When $S \leq S_p$, the new relative permeability of water is,

$$k_w = \frac{K_w}{K_0} = \tau^{1/2}[\frac{\int_0^r \delta\beta rf(r)dr}{\int_0^\infty rf(r)dr}]^2 = \tau^{1/2}[\delta\beta F(\bar{S})]^2, \tag{23}$$

where $\tau = \delta^2\bar{S}$.

Thus, the ratio of the new water relative permeability over the initial water relative permeability is,

$$\frac{k_w}{k_{w0}} = \delta^3\beta^2. \tag{24}$$

When $S > S_p$,

$$k_w = \frac{K_w}{K_0} = \tau^{1/2}[\frac{\int_0^{r_p} \delta\beta rf(r)dr + \int_{r_p}^r rf(r)dr}{\int_0^\infty rf(r)dr}]^2 = \tau^{1/2}[F(\bar{S}) + (\delta\beta - 1)F(\bar{S}_p)]^2, \tag{25}$$

where $\tau = \delta^2\bar{S}_p + \bar{S} - \bar{S}_p$.

Thus,

$$\frac{k_w}{k_{w0}} = (\frac{\bar{S} - \bar{S}_p + \delta^2\bar{S}_p}{\bar{S}})^{1/2}[\frac{F(\bar{S}) + (\delta\beta - 1)F(\bar{S}_p)}{F(\bar{S})}]^2. \tag{26}$$

To summarize, the new relation between relative permeability of the wetting phase and precipitation is:

$$\frac{k_w}{k_{w0}} = \begin{cases} \delta^3\beta^2 & S \leq S_p \\ (\frac{\bar{S} - \bar{S}_p + \delta^2\bar{S}_p}{\bar{S}})^{1/2}[\frac{F(\bar{S}) + (\delta\beta - 1)F(\bar{S}_p)}{F(\bar{S})}]^2 & S > S_p \end{cases}. \tag{27}$$

3.5. Relative Permeability of Non-Wetting Phase

Van Genuchten (1980) did not give the explicit formulation for the relative permeability of non-wetting phase as a function of effective water saturation, but it is straightforward to derive this given the discussions above. Again, we denote the initial permeability of the non-wetting phase as K_{g0}, relative permeability as k_{g0}, and the new permeability of the non-wetting phase as K_g, relative permeability as k_g. The integration for the relative permeability of non-wetting phase is from r to ∞:

$$k_{g0} = \frac{K_{g0}}{K_0} = \tau^{1/2}[\frac{\int_r^\infty rf(r)dr}{\int_0^\infty rf(r)dr}]^2 = \tau^{1/2}[1 - F(\bar{S})]^2, \tag{28}$$

where $\tau = 1 - \bar{S}$.

When $S \leq S_p$, the new relative permeability of non-wetting phase is,

$$k_g = \frac{K_g}{K_0} = \tau^{1/2}[\frac{\int_r^{r_p} \delta\beta rf(r)dr + \int_{r_p}^\infty rf(r)dr}{\int_0^\infty rf(r)dr}]^2 = \tau^{1/2}[1 - \delta\beta F(\bar{S}) + (\delta\beta - 1)F(\bar{S}_p)]^2, \tag{29}$$

where $\tau = (\bar{S}_p - \bar{S})\delta^2 + (1 - \bar{S}_p)$.

Thus,

$$\frac{k_g}{k_{g0}} = [\frac{(\bar{S}_p - \bar{S})\delta^2 + (1 - \bar{S}_p)}{1 - \bar{S}}]^{1/2}[\frac{1 - \delta\beta F(\bar{S}) + (\delta\beta - 1)F(\bar{S}_p)}{1 - F(\bar{S})}]^2. \tag{30}$$

When $S > S_p$,

$$k_g = \frac{K_g}{K_0} = \tau^{1/2}[\frac{\int_r^\infty rf(r)dr}{\int_0^\infty rf(r)dr}]^2 = \tau^{1/2}[1 - F(\bar{S})]^2, \tag{31}$$

where $\tau = 1 - \bar{S}$.

Thus,

$$\frac{k_g}{k_{g0}} = 1. \tag{32}$$

To summarize, the new relation between relative permeability of the non-wetting phase and precipitation is:

$$\frac{k_g}{k_{g0}} = \begin{cases} [\frac{(\bar{S}_p - \bar{S})\delta^2 + (1 - \bar{S}_p)}{1 - \bar{S}}]^{1/2}[\frac{1 - \delta\beta F(\bar{S}) + (\delta\beta - 1)F(\bar{S}_p)}{1 - F(\bar{S})}]^2 & S \leq S_p \\ 1 & S > S_p \end{cases}. \tag{33}$$

4. Verification with Pore Network Modeling

In order to test the new equations for calculating changes of capillary pressure and relative permeabilities due to mineral precipitation and dissolution, we use pore network modeling (PNM) to compute these functions in a two-phase flow system. The model comprises a constrained set of parameters that mimic the pore structure of a porous medium.

PNM is commonly used to predict capillary pressure and relative permeability functions for multi-phase flow simulations, and uses idealized geometric representations of complex pore structures and principles of percolation/invasion theory (Blunt, 2001; Blunt et al., 2013). It is a well-established approach for calculating the small-scale petrophysical functions of two- and three-phase flow through porous media. Here we use the pore-network model of Ryazanov et al. (2009). This model can be applied to complex unstructured pore-networks, considers film and layer-flow using thermodynamic criteria, uses a variety of shapes to represent the shapes of the pore throats, and has been extensively validated using experimental data.

4.1. Initial Pore Network Model

We use a realistic 3D pore-network extracted from pore-space reconstruction methods and CT images that are geometrically and topologically equivalent to the pore structures of a Berea sandstone sample (Fig.3). The network consists of 12349 pores bodies (nodes) and 26146 pore throats (bonds). Each pore is assigned a regular shape (triangle, star, or circle) based on the shape factor which best matches that of the real pore shape. The average coordination number of this pore network is 4.19, initial permeability is 1639.47 mD, and porosity is 0.24. In this numerical experiment, we start with a fully water-saturated network ($S = 1.0$). Then, the non-wetting phase is injected into the network for primary drainage. The pore network model calculates the capillary pressure curve and relative permeability curves as a function of water saturation through flooding. All floods are assumed to be capillary dominated and are simulated according to invasion-percolation principles.

The initial capillary pressure curve and relative permeability curves are shown in Fig.4 and Fig.5 for this pore network. They are calculated by running primary drainage of non-wetting phase through an initially water-saturated sample. As can be determined in Fig.4 and Fig.5, the residual saturation of water is 0.24.

In order to determine a reasonable value for the parameter m, we use Eq.3 to fit the capillary pressure curve in Fig.4. Resulting parameters from fitting the capillary pressure curve are $m = 0.748, \alpha = 0.0001994 Pa^{-1}$. To test this m value on the relative permeability curves, we used Eq.6 and compared results with the relative permeabilities calculated from pore network modeling. Results show that the van Genuchten/Mualem model presents a satisfactory fit of initial capillary pressure and

relative permeability curves. We then use the value of m to predict how the capillary pressure curve and relative permeabilities change after chemical reactions, for a given amount of dissolved/precipitated minerals. The new capillary pressure and relative permeabilities are calculated from the initial values and the modification factors from our relations. The fitted initial van Genuchten/Mualem curves are not used in these calculation, thus do not affect the results. The main objective in the fitting process is to obtain the value of m which contains information on the shape of pore size distribution function, and is used in the relations.

4.2. Porosity-Permeability Relationship

For the purpose of comparing pore network modeling results with the new closed-form equations, we select two water saturations of 0.5 and 1.0 as the saturations at which mineral dissolution/precipitation occurs. Here we refer the two cases as the 'new approach' and the 'traditional approach' respectively since traditionally the relation between flow properties and chemical reactions are built on the assumption of full water saturation. In the new approach, we use the pore network model and run a primary drainage from the initial water-saturated condition to the target water saturation of 0.5. The bonds and nodes that are filled with water were identified in the pore network model when water saturation reaches $S_p = 0.5$. As shown in Fig.3, the red is the invaded non-wetting phase at $S_p = 0.5$, while the blue is water. Subsequently, the radii of the water-occupied bonds and nodes were modified by a factor of δ according to Eqs.7 and 9 for a given porosity change. In the traditional approach, the pore radii of all pores and throats are modified in the pore network model given the same amount of porosity change. This corresponds to the traditional assumption in which chemical reactions are considered to occur in all pores. The modified pore network models using both approaches were flooded again with non-wetting phase starting from a fully water saturated condition to calculate the new permeability, capillary pressure and relative permeability curves.

Fig.6 shows permeabilities of modified pore network models as a function of porosity change using the two approaches. The values of β are calculated from the porosity change using Eq.8 where $S_p = 0.5, \phi_0 = 0.24$. Given that $\beta \geq 0$, we have $\phi_{min}/\phi_0 = 1 - S_p = 0.5$, which means that porosity cannot drop below 50% of its original value given $S_p = 0.5$, because precipitation cannot be more than available pore volume. Ideally porosity does not have an upper limit due to dissolution. However, since the current work only considers the change in pore size, it will not be valid when the porosity increase is large and pore structure is heavily modified. In fact, there will probably be wormholes forming when porosity increases substantially, which has not yet been well modeled. For the range of porosity depicted in Fig.6 (0.19-0.27), the value of β ranges from 0.583 to 1.25, and the value of δ ranges from 0.088 to 2.73.

In Fig.6 it can be observed that using the traditional approach in which precipitation is assumed to happen in all pores and throats, permeability decreases up to 3 orders of magnitude when porosity decreases from 0.24 to 0.19. However, if precipitation is limited in the water occupied pores and throats, only the radii of the small pores and throats are decreased, while the other pores and throats remain unchanged. Thus permeability converges to a value which corresponds to all the unchanged pores and throats and does not decrease to zero. This is well captured by the present model, which we refer to as the modified Liu et al. (2013) model because the Liu et al. (2013) model only considered the change in radius but not in volume of the pores after mineral reactions as discussed in Section 3. The permeability change can be characterized into two regions, a transitional stage from porosity 0.24 to 0.22, and a plateau where permeability is relatively constant when porosity is smaller than 0.22. Most of the permeability is contributed from the unchanged pores and throats on this plateau. The traditional method which assumes that all pores and throats are filled by precipitations fails to capture this result.

4.3. Capillary Pressure and Relative Permeabilities

The predicted capillary pressure and relative permeabilities from pore network calculations are compared with our model in Figs.7-12. Two sets of calculations were conducted and compared. The first set of calculations assumes a decrease of porosity from 0.24 to 0.2015 ($\beta = 0.6795, \delta = 0.1757$), which represents precipitation, and the second set of calculations increases porosity from 0.24 to 0.2592 ($\beta = 1.160, \delta = 1.952$), which represents dissolution. The dashed lines in all figures are the initial capillary pressure or relative permeabilities. The solid lines represent predictions from our current model and the dots are results from pore network modeling. The initial PNM data is used directly in our model and modifications of this data are applied after dissolution or precipitation based on our new relations.

In Fig.7, capillary pressure is increased by a factor of $1/\delta$ for water saturation smaller than 0.5,using the new approach, while remains unchanged for water saturation larger than 0.5, according to Eq.11. Thus, there is an offset at $S_w = 0.5$ that is well captured by our model and the pore network calculation. In Fig.8, the relative permeability of water is decreased by a factor of $\delta^3\beta^2$ for $S_w < 0.5$ according to Eq.27. Again, there is an offset at $S_w = 0.5$, and the change of relative permeability is less substantial for $S_w > 0.5$. The relative permeability of non-wetting phase in Fig.9 is unchanged for $S_w > 0.5$, but reduced for $S_w < 0.5$ according to Eq.33.

Fig.10-Fig.12 show the capillary pressure and relative permeability changes in the dissolution case, and the results from pore network models are well captured by our closed-form equations. Note that the relations of how relative permeabilities change after mineral dissolution is not given explicitly in this work, due to the fact that capillary pressure head cannot be written as an explicit function of water saturation

(Eq.14). In Fig.11 and 12 we adopted the relations for relative permeabilities in the precipitation case (Eq.27 and 33), and these relations fit the PNM data relatively well. In fact, Eq. 27 and 33 are valid in the dissolution case for $S < S_1$ and $S > S_2$ (Fig.2), since the $Pc - S$ relations are the same for dissolution and precipitation in these two regions. However, the interpolation between S_1 and S_2 will be slightly different. For permeability, the relation in the dissolution case is identical to the precipitation case. In the dissolution case, the pore sizes need to be rearranged to be consistent with the order of capillary tubes filled by water, from small to large. However, since permeability is calculated by integrating through all capillary tubes, the rearrangement does not affect the result. Thus the closed form relation for permeability change in the precipitation case can be directly used in the dissolution case.

In summary, the comparisons indicate that our proposed continuum-scale relations satisfactorily predict the pore-scale modeling results. The new method enables calculations of new permeability, capillary pressure and relative permeabilities in reservoir simulators after mineral reactions. It includes parameters that describe pore size distribution (m), the fraction of pore space that is water filled when precipitation happens (S_p), and the amount of precipitation/dissolution (δ, β). The related parameters are either model input (e.g., m), or intermediate modeling results (e.g., S_p), for calculating two-phase flow, so no new parameters need to be defined in reservoir simulators or reactive transport codes.

5. Discussions and Conclusions

The capillary tube model, which is the foundation of the presented model, has several underlying assumptions (Larson et al., 1981). One is that the connectivity of real porous media and the irregular geometry of real porous matrices and associated effects are ignored. Also this model neglects the water wetting films in pores filled by a non-wetting phase. Hence we cannot model how chemical components diffuse through these water films and eventually react with a (small) fraction of the pore space. Despite these shortcomings, the capillary tube model is widely applied as a simple link between continuum-scale hydraulic properties and PSD's (Taylor and Jaffé, 1990). In this paper we integrate the concept of modifying pore volumes through mineral reactions into more sophisticated pore network models to relate PSD's to capillary pressure curve and relative permeabilites. Comparisons between our capillary tube model and pore network model show that satisfactory predictions can be achieved using the capillary tube model for changes in capillary pressure, permeability and relative permeabilites.

The main contribution in this paper is the advancement of continuum-scale models for the effect of chemical reactions on multi-phase flow properties. One key step in reactive transport modeling is to capture these effects for feedbacks of chemical

reaction on fluid flow. Currently in most reactive transport simulators this is limited to estimating permeability change from porosity change. However, due to the fact that permeability is not a single function of porosity, but also a function of pore geometry, the current approach has large uncertainties. In this paper, we adopt the Liu et al. (2013) model for permeability change which not only considers porosity change but also takes into account pore size distribution and water saturation. We extend the Liu et al. (2013) model to multi-phase flow properties, and provide closed-form equations on how capillary pressure and relative permeabilities should change due to chemical reactions. These relations are continuum-scale equations, and can be implemented in reactive transport models directly without introducing additional parameters.

References

Algive, L., Békri, S., Nader, F. H., Lerat, O., Vizika, O., 2012. Impact of diagenetic alterations on the petrophysical and multiphase flow properties of carbonate rocks using a reactive pore network modeling approach. Oil & Gas Science and Technology–Revue dIFP Energies nouvelles 67 (1), 147–160.

Bjørkum, P. A., Nadeau, P. H., 1998. Temperature controlled porosity/permeability reduction, fluid migration, and petroleum exploration in sedimentary basins. APPEA Journal 38 (Part 1), 452–464.

Blunt, M. J., 2001. Flow in porous mediapore-network models and multiphase flow. Current opinion in colloid & interface science 6 (3), 197–207.

Blunt, M. J., Bijeljic, B., Dong, H., Gharbi, O., Iglauer, S., Mostaghimi, P., Paluszny, A., Pentland, C., 2013. Pore-scale imaging and modelling. Advances in Water Resources 51, 197–216.

Brace, W., 1977. Permeability from resistivity and pore shape. Journal of Geophysical Research 82 (23), 3343–3349.

Carman, P. C., 1956. Flow of gases through porous media. Academic press.

Ginn, T. R., Wood, B. D., Nelson, K. E., Scheibe, T. D., Murphy, E. M., Clement, T. P., 2002. Processes in microbial transport in the natural subsurface. Advances in Water Resources 25 (8), 1017–1042.

Hiorth, A., Cathles, L., Madland, M., 2010. The impact of pore water chemistry on carbonate surface charge and oil wettability. Transport in porous media 85 (1), 1–21.

Kozeny, J., 1927. Über kapillare Leitung des Wassers im Boden:(Aufstieg, Versickerung und Anwendung auf die Bewässerung). Hölder-Pichler-Tempsky.

Larson, R., Scriven, L., Davis, H., 1981. Percolation theory of two phase flow in porous media. Chemical Engineering Science 36 (1), 57–73.

Li, L., Peters, C. A., Celia, M. A., 2006. Upscaling geochemical reaction rates using pore-scale network modeling. Advances in water resources 29 (9), 1351–1370.

Liu, H.-H., Zhang, G., Yi, Z., Wang, Y., 2013. A permeability-change relationship in the dryout zone for co_2 injection into saline aquifers. International Journal of Greenhouse Gas Control 15, 42–47.

Mavis, F., Wilsey, E., 1937. Filter sand permeability studies. Eng. News Rec 118, 299–300.

Mualem, Y., 1976. A new model for predicting the hydraulic conductivity of unsaturated porous media. Water Resour. Res 12 (3), 513–522.

Nogues, J. P., Fitts, J. P., Celia, M. A., Peters, C. A., 2013. Permeability evolution due to dissolution and precipitation of carbonates using reactive transport modeling in pore networks. Water Resources Research 49 (9), 6006–6021.

Ott, H., Roels, S., De Kloe, K., 2015. Salt precipitation due to supercritical gas injection: I. capillary-driven flow in unimodal sandstone. International Journal of Greenhouse Gas Control 43, 247–255.

Panda, M. N., Lake, L. W., 1995. A physical model of cementation and its effects on single-phase permeability. AAPG bulletin 79 (3), 431–443.

Pruess, K., Müller, N., 2009. Formation dry-out from co2 injection into saline aquifers: 1. effects of solids precipitation and their mitigation. Water Resources Research 45 (3).

Raoof, A., Nick, H., Hassanizadeh, S., Spiers, C., 2013. Poreflow: A complex pore-network model for simulation of reactive transport in variably saturated porous media. Computers & Geosciences 61, 160–174.

Ritter, H., Drake, L., 1945. Pressure porosimeter and determination of complete macropore-size distributions. pressure porosimeter and determination of complete macropore-size distributions. Industrial & Engineering Chemistry Analytical Edition 17 (12), 782–786.

Ryazanov, A., Van Dijke, M., Sorbie, K., 2009. Two-phase pore-network modelling: existence of oil layers during water invasion. Transport in Porous Media 80 (1), 79–99.

Schäfer, D., Schäfer, W., Kinzelbach, W., 1998. Simulation of reactive processes related to biodegradation in aquifers: 1. structure of the three-dimensional reactive transport model. Journal of contaminant Hydrology 31 (1), 167–186.

Schechter, R., Gidley, J., 1969. The change in pore size distribution from surface reactions in porous media. AIChE Journal 15 (3), 339–350.

Steefel, C. I., DePaolo, D. J., Lichtner, P. C., 2005. Reactive transport modeling: An essential tool and a new research approach for the earth sciences. Earth and Planetary Science Letters 240 (3), 539–558.

Taylor, S. W., Jaffé, P. R., 1990. Biofilm growth and the related changes in the physical properties of a porous medium: 1. experimental investigation. Water Resources Research 26 (9), 2153–2159.

Van Genuchten, M. T., 1980. A closed-form equation for predicting the hydraulic conductivity of unsaturated soils. Soil science society of America journal 44 (5), 892–898.

Varloteaux, C., Békri, S., Adler, P. M., 2013. Pore network modelling to determine the transport properties in presence of a reactive fluid: From pore to reservoir scale. Advances in Water Resources 53, 87–100.

Verma, A., Pruess, K., 1988. Thermohydrological conditions and silica redistribution near high-level nuclear wastes emplaced in saturated geological formations. Journal of Geophysical Research: Solid Earth (1978–2012) 93 (B2), 1159–1173.

Xie, M., Mayer, K. U., Claret, F., Alt-Epping, P., Jacques, D., Steefel, C., Chiaberge, C., Simunek, J., 2014. Implementation and evaluation of permeability-porosity and tortuosity-porosity relationships linked to mineral dissolution-precipitation. Computational Geosciences, 1–17.

Nomenclature

$\bar{S}$ Effective water saturation

β Ratio of pore volume after reactions to before reactions

534	ϕ	Porosity after reactions
535	ϕ_0	Initial porosity
536	τ	Tortuosity
537	h	Capillary pressure head
538	K	Permeability after reactions
539	K_0	Initial permeability
540	K_{g0}	Initial gas permeability
541	k_{g0}	Initial gas relative permeability
542	K_g	Gas permeability after reactions
543	k_g	Gas relative permeability after reactions
544	K_{w0}	Initial water permeability
545	k_{w0}	Initial water relative permeability
546	K_w	Water permeability after reactions
547	k_w	Water relative permeability after reactions
548	m	Empirical parameter in the van Genuchten $h - S$ relation
549	r	Radius of capillary tube
550	r^*	Radius after reactions
551	r_p	Maximum radius up to which pores are water-filled
552	S	Water saturation
553	S_p	Water saturation when mineral reaction occurs
554	S_r	Residual water saturation

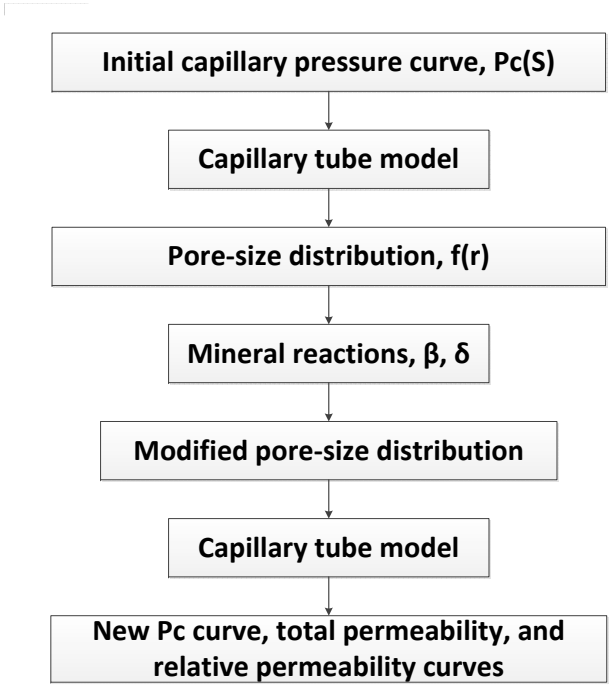

Figure 1: Work flow to develop new constitute relations for multi-phase flow properties and chemical reactions.

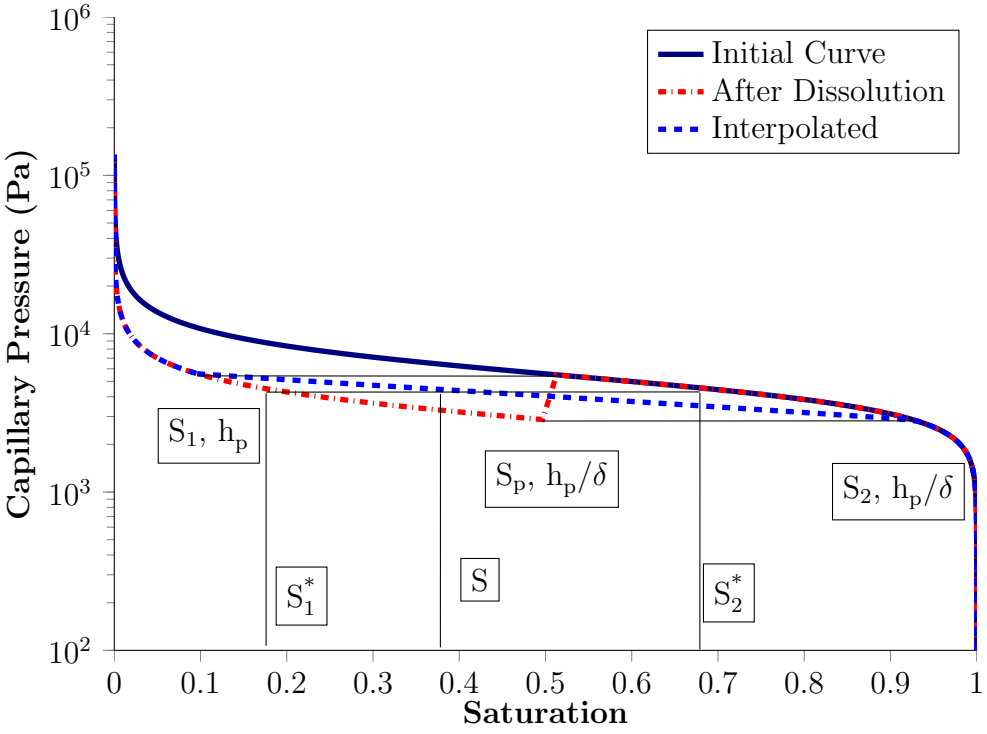

Figure 2: Change of capillary pressure curve after mineral dissolution. Red dash-dot line illustrates the approach used in the precipitation case, which gives un-physical results in the dissolution case. Blue dashed line represents the correct new capillary pressure curve as discribed by Eq.14. For any capillary pressure head h on the new curve, its saturation S can be determined from volume balance (Eq.13).

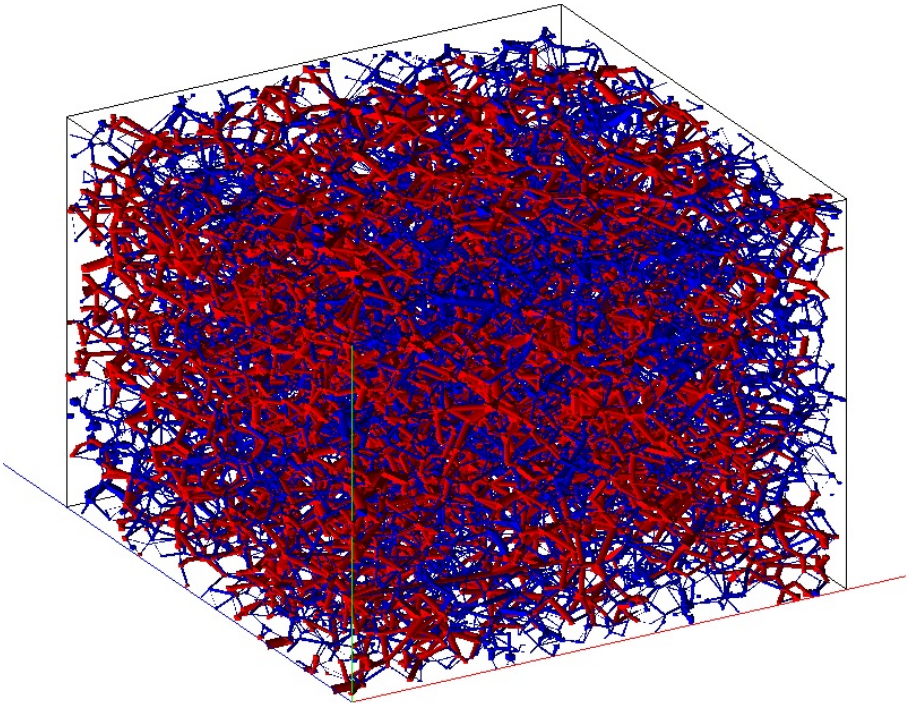

Figure 3: Snap shot of the Berea pore network model at water saturation of 0.5. Blue color represents water, red color represents the non-wetting phase. Size of the model is 2.14 mm x 2.14 mm x 2.14 mm.

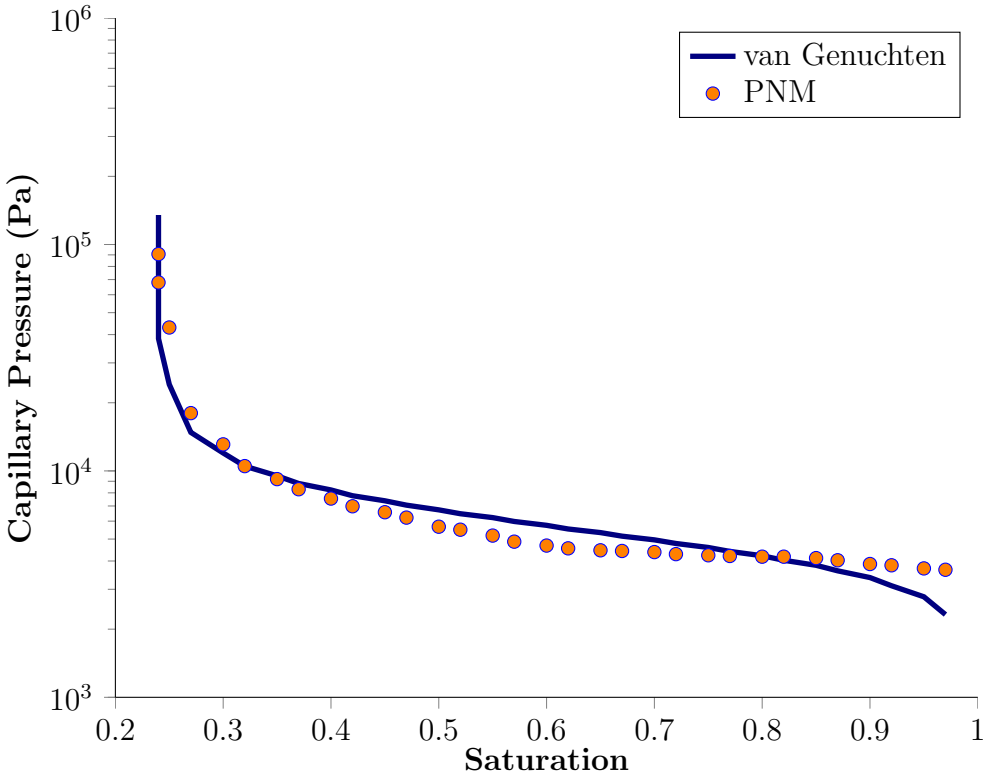

Figure 4: Initial capillary pressure data from pore network modeling and fitting with van Genuchten relation.

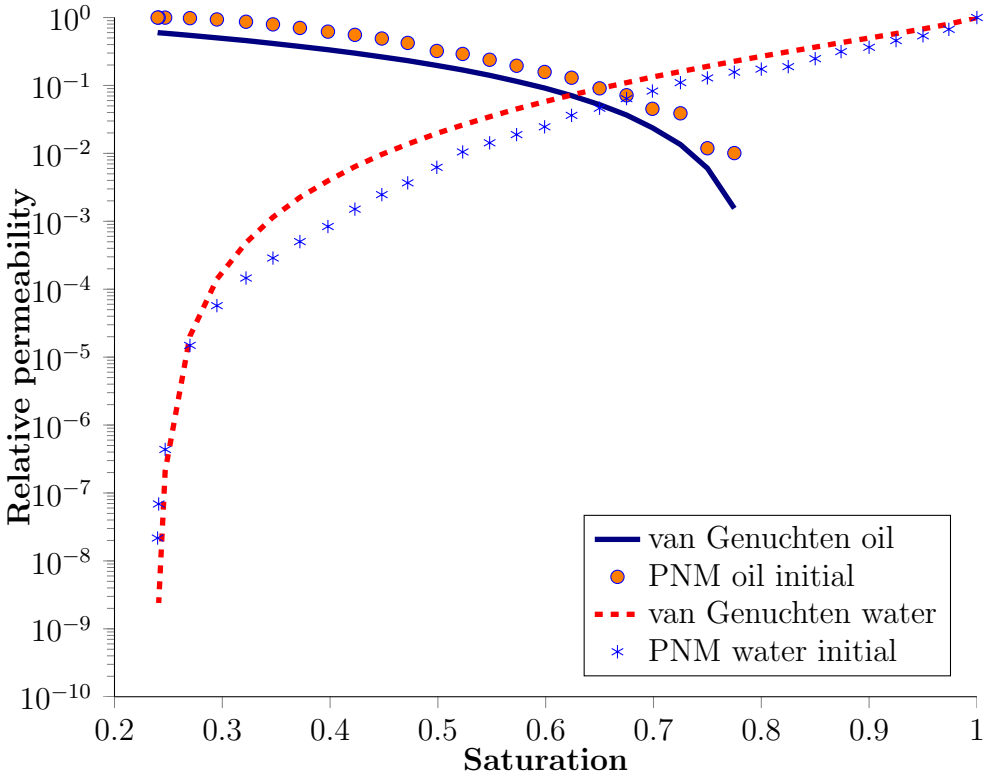

Figure 5: Initial relative permeabilities of water and non-wetting phase from pore network modeling and comparison with van Genuchten relations using parameters from 4.

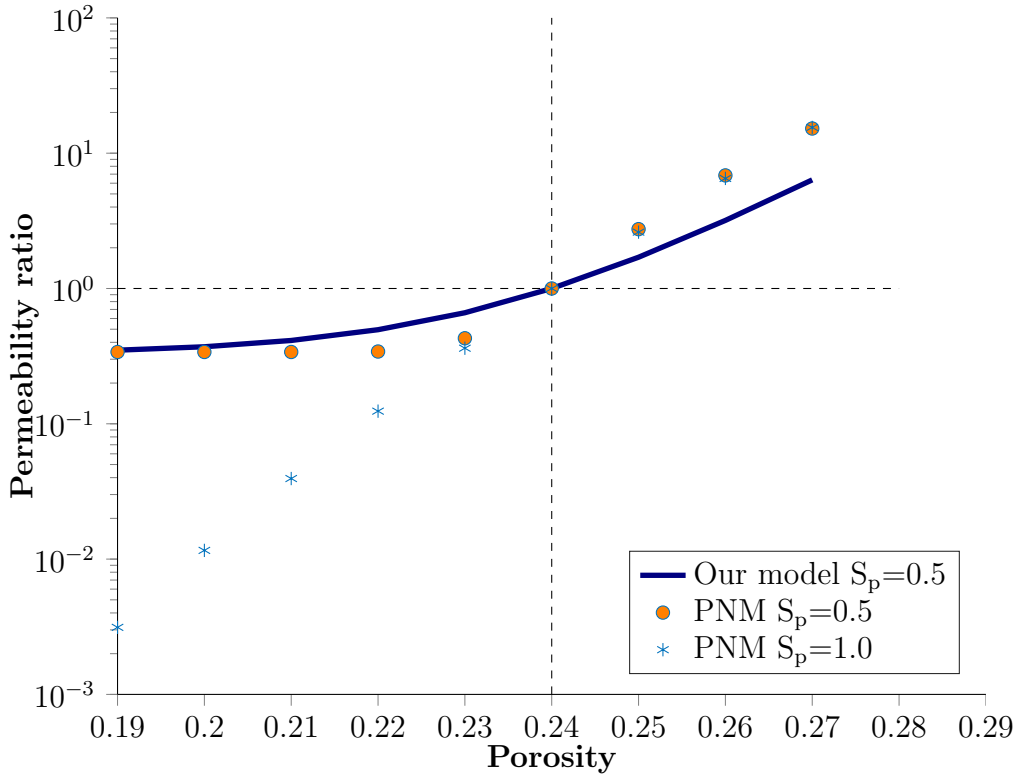

Figure 6: Permeability change as a function of porosity change predicted from current model and pore network modeling ($S_p = 0.5$), compared with tranditional approach where all pores and throats are assumed to have chemical reactions ($S_p = 1.0$). In our model, $S_p = 0.5, \phi_0 = 0.24$, the value of β ranges from 0.583 to 1.25, and the value of δ ranges from 0.088 to 2.73.

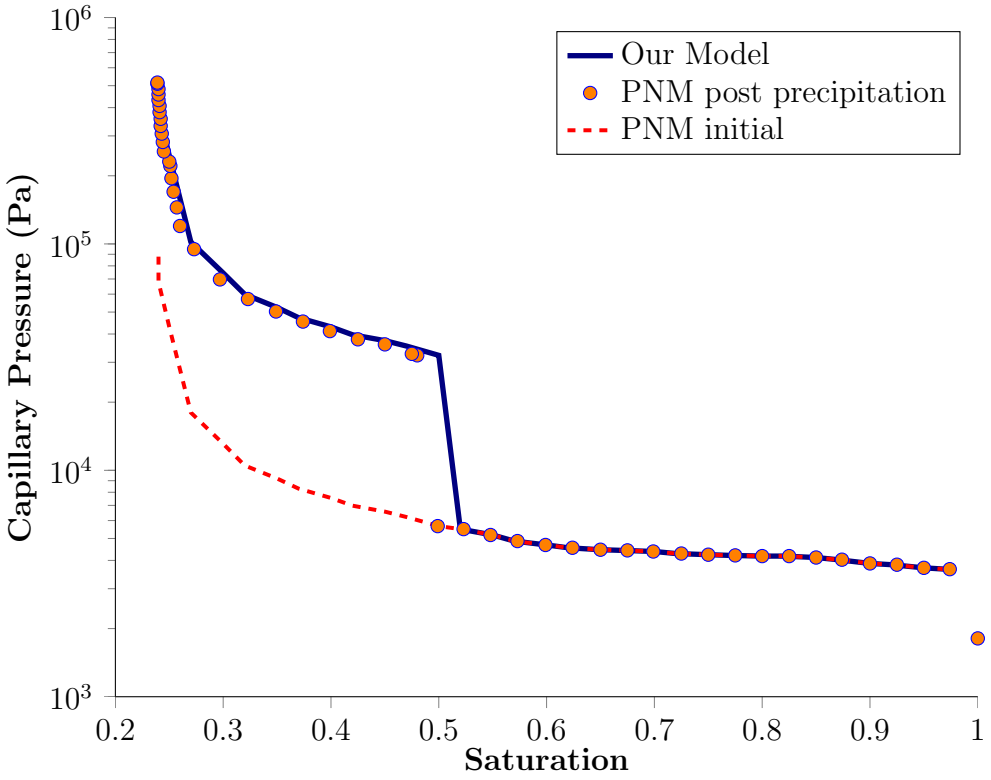

Figure 7: New capillary pressure curve after mineral precipitation predicted from our model and comparison with pore network modeling, using the new approach.

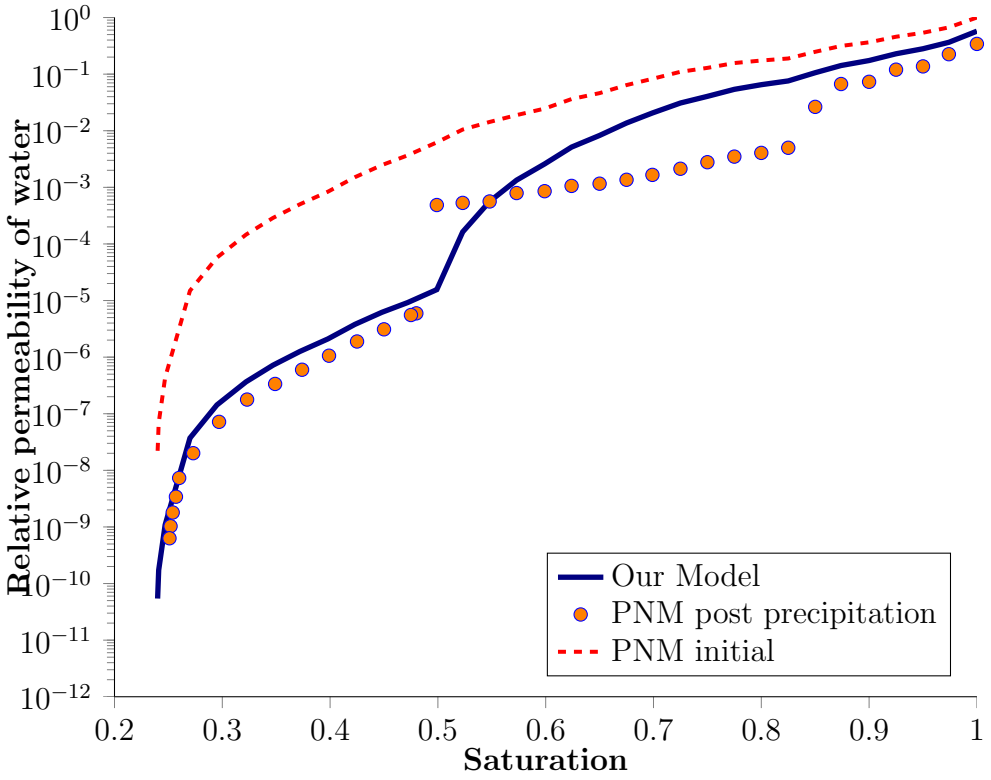

Figure 8: New water relative permeability curve after mineral precipitation predicted from our model and comparison with pore network modeling, using the new approach.

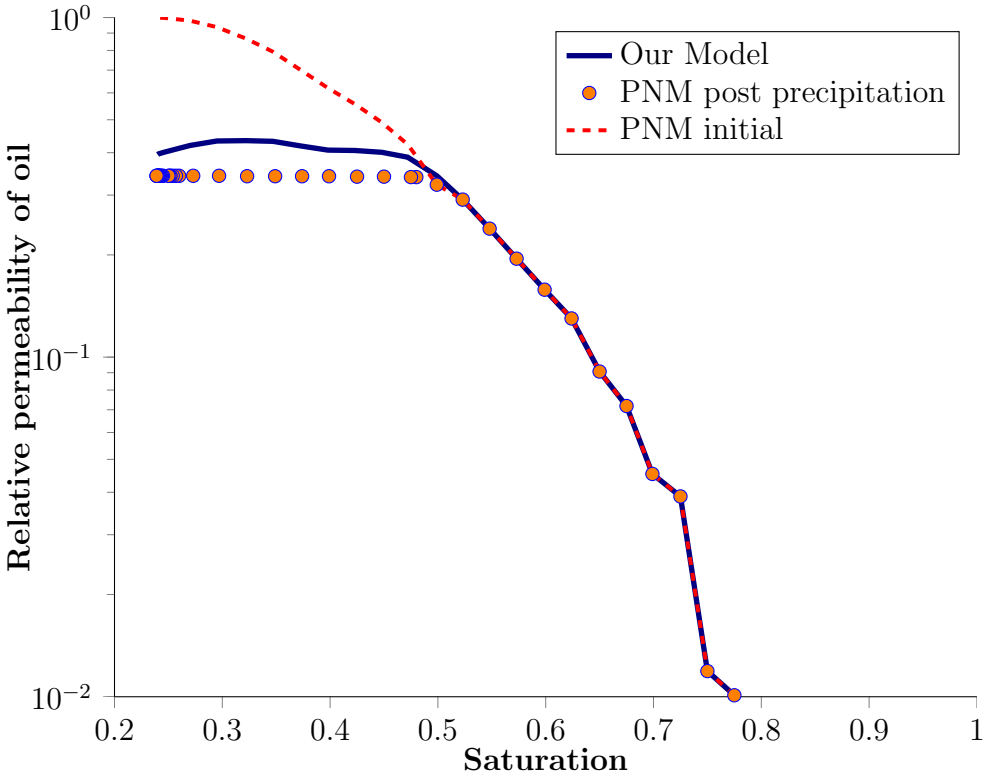

Figure 9: New relative permeability of the non-wetting phase after mineral precipitation predicted from our model and comparison with pore network modeling, using the new approach.

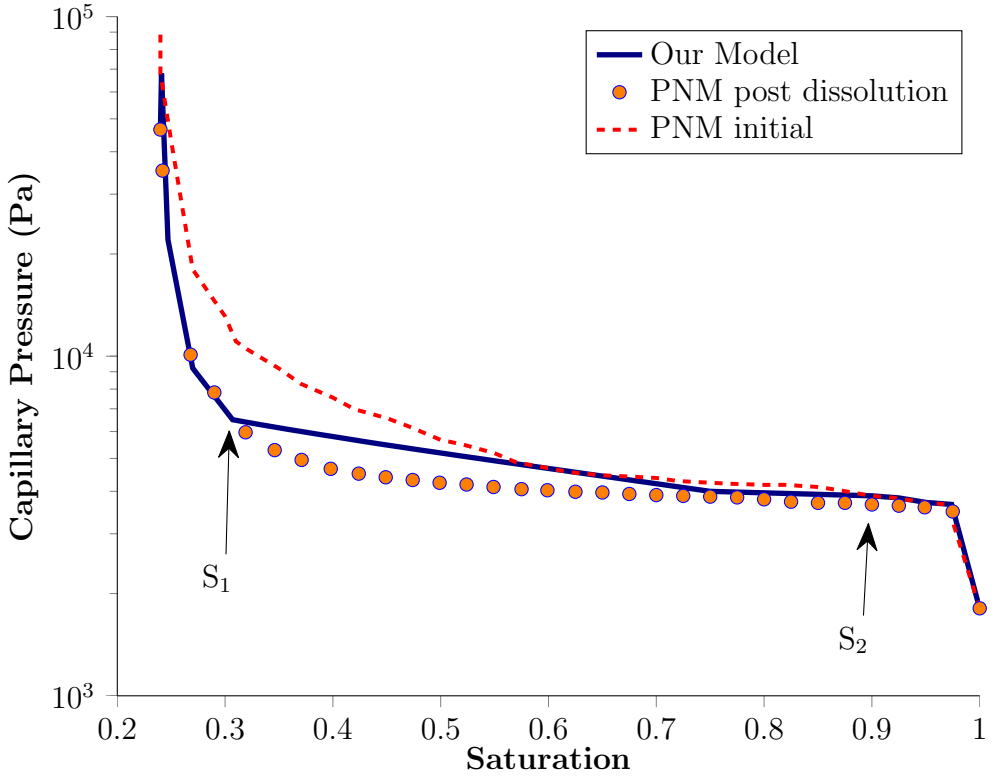

Figure 10: New capillary pressure curve after mineral dissolution predicted from our model and comparison with pore network modeling, using the new approach.

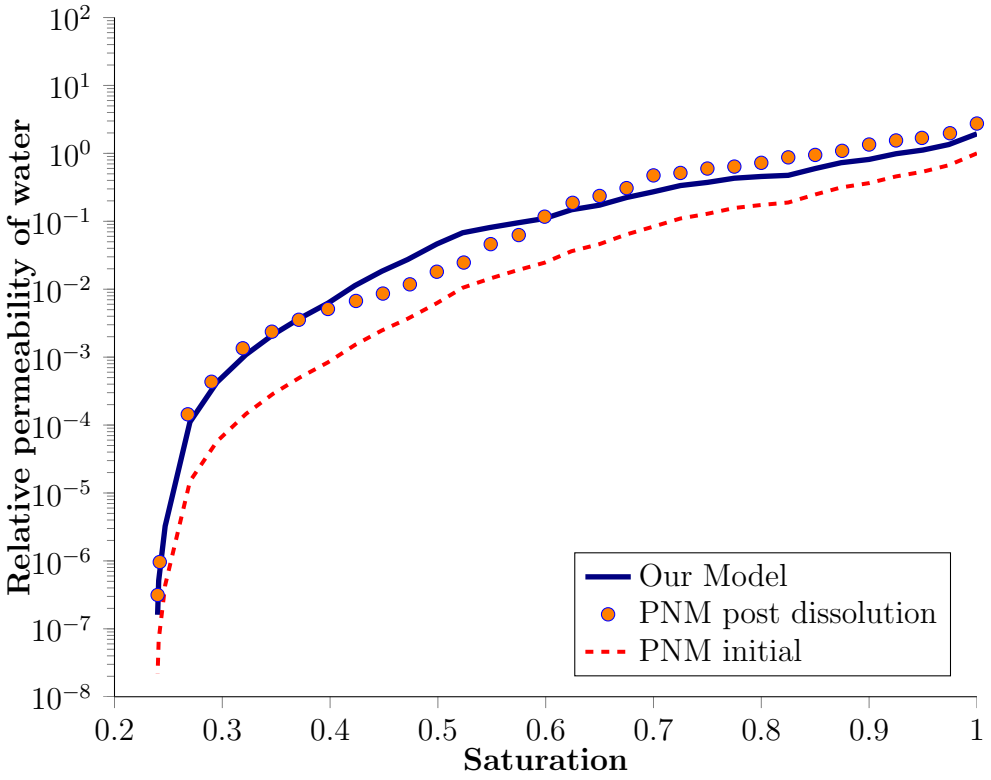

Figure 11: New water relative permeability curve after mineral dissolution predicted from our model and comparison with pore network modeling, using the new approach.

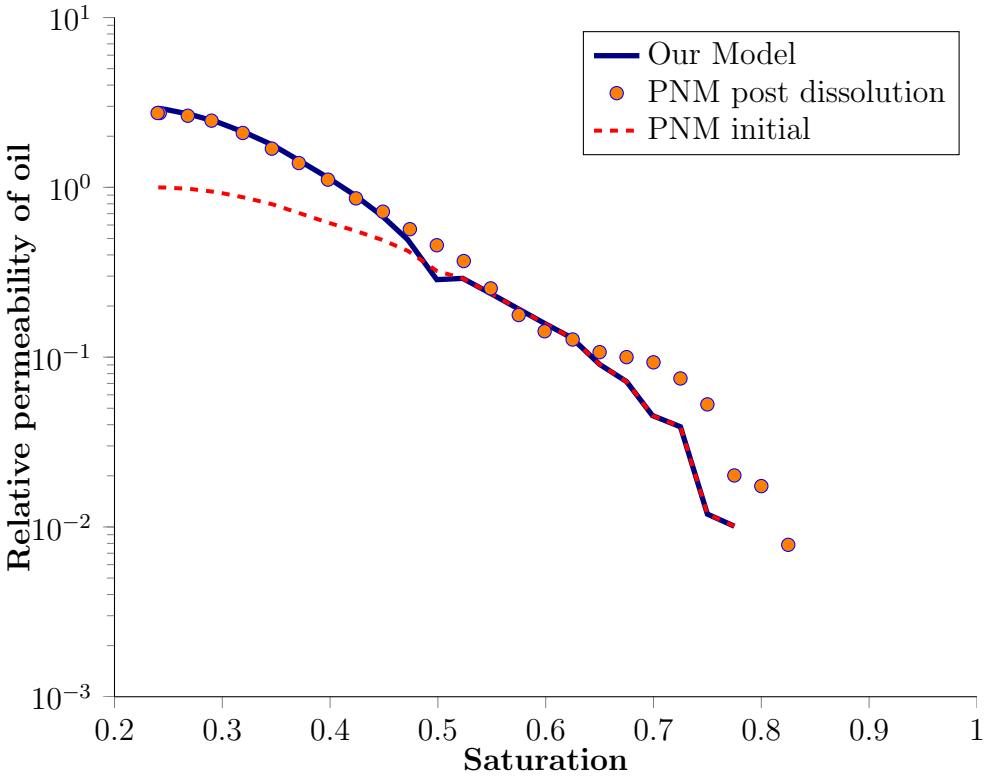

Figure 12: New relative permeability curve of the non-wetting phase after mineral dissolution predicted from our model and comparison with pore network modeling, using the new approach.